GEOLOGY | THE GEOLOGICAL SOCIETY OF AMERICA®

https://doi.org/10.1130/G48861.1

Manuscript received 14 October 2020
Revised manuscript received 25 January 2021
Manuscript accepted 18 March 2021

Published online 17 May 2021

Evidence for iron-rich sulfate melt during magnetite(-apatite) mineralization at El Laco, Chile

Wyatt M. Bain[1], Matthew Steele-MacInnis[1]*, Fernando Tornos[2,3], John M. Hanchar[3], Emily C. Creaser[1] and Dorota K. Pietruszka[3]

[1]Department of Earth and Atmospheric Sciences, University of Alberta, Edmonton, Alberta T6G 2E3, Canada
[2]Instituto de Geociencias (IGEO, CSIC-UCM), Dr Severo Ochoa, 7, 28040 Madrid, Spain
[3]Department of Earth Sciences, Memorial University of Newfoundland, St. John's, Newfoundland A1B 3X5, Canada

ABSTRACT

The origins of Kiruna-type magnetite(-apatite) [Mt(-Ap)] deposits are contentious, with existing models ranging from purely hydrothermal to orthomagmatic end members. Here, we evaluate the compositions of fluids that formed the classic yet enigmatic Mt(-Ap) deposit at El Laco, northern Chile. We report evidence that ore-stage minerals crystallized from an Fe-rich (6–17 wt% Fe) sulfate melt. We suggest that a major component of the liquid was derived from assimilation of evaporite-bearing sedimentary rocks during emplacement of andesitic magma at depth. Hence, we argue that assimilation of evaporite-bearing sedimentary strata played a key role in the formation of El Laco and likely Mt(-Ap) deposits elsewhere.

INTRODUCTION

"Kiruna-type" magnetite-(apatite) [Mt(-Ap)] deposits (referring to the deposit at Kiruna, Sweden) are major resources of iron, but their genesis is vigorously debated. Some argue for a hydrothermal origin, whereby veins, breccias, and replacement zones are formed by circulation of hot aqueous fluids of magmatic or basinal derivation (Hildebrand, 1986; Rhodes and Oreskes, 1999; Sillitoe and Burrows, 2002). Others argue for an orthomagmatic origin, whereby orebodies are formed by emplacement and crystallization of Fe-rich silicate melt or immiscible iron-oxide melt (Nyström and Henriquez, 1994; Naslund et al., 2002; Velasco et al., 2016; Mungall et al., 2018). Some models invoke combinations of magmatic and hydrothermal processes, including exsolution of brines from Fe-rich melts (Tornos et al., 2017) or buoyancy-driven flotation of magmatic magnetite by aqueous fluids (Knipping et al., 2015; Simon et al., 2018). Yet, the compositions of the ore-forming fluids—whether aqueous, silicate, oxide, or other—remain unclear. A recent study of two Mt(-Ap) systems in the southwestern United States showed that Fe-rich (~4–14 wt% Fe) carbonate-sulfate melts were present throughout the paragenesis of those systems (Bain et al., 2020). This raises the possibility that carbonate-sulfate melts play a key role in Mt(-Ap) systems. We test whether similar melts played a role in mineralization at the El Laco deposit in northern Chile (Fig. 1).

The El Laco system (Fig. 1) is central to the current debate about Mt(-Ap) genesis because it shows (1) exceptionally well-preserved volcanic textures suggesting an orthomagmatic (subaerial volcanic) origin, and (2) widespread Na-K-Ca alteration suggestive of hydrothermal processes (Tornos et al., 2017). Both types of features have been invoked as evidence for a range of contrasting orthomagmatic and hydrothermal models, which are difficult to reconcile. These competing models for El Laco epitomize the wider debate about Mt(-Ap) genesis globally.

We characterize the ore-forming fluids at El Laco by detailed analyses of inclusions hosted in ore-stage diopside-magnetite-anhydrite veins from the Pasos Blancos orebody (Fig. 1; Table S1 in the Supplemental Material[1]). We focus on assemblages of primary inclusions, and our results show that an Fe-rich sulfate melt was present during magnetite deposition. Hence, we argue that sulfate-rich melts drove mineralization at El Laco and are likely common to Mt(-Ap) systems more broadly.

GEOLOGIC CONTEXT

El Laco is a Pliocene (5.3–1.6 Ma; Naranjo et al., 2010) stratovolcano consisting of radially distributed andesite flows (Naslund et al., 2002; Tornos et al., 2017) that are isotopically indistinguishable from those of the nearby Lascar volcano (Matthews et al., 1994) and other volcanoes in the Central Volcanic Zone (CVZ) of South America (Harmon et al., 1984; Richards and Villeneuve, 2001). El Laco is underlain by thick sedimentary sequences that include limestones and sulfate evaporites of the Cretaceous–Tertiary Salta Group (Matthews et al., 1996; Marquillas et al., 2005; Tornos et al., 2017) and phosphatic siderite ironstones of the Paleozoic basement (Boso and Monaldi, 1990; Mungall et al., 2018). The presence of these lithologies at depth likely accounts for significant crustal contamination of the intruding andesites (Harmon et al., 1984; Matthews et al., 1994) and the strong crustal Sr-Nd signature of the Mt(-Ap) orebodies (Tornos et al., 2017).

Magnetite(-apatite) mineralization at El Laco occurs mostly as stratabound orebodies interbedded with andesite flows (Naslund et al., 2002; Tornos et al., 2017). The orebodies are fed by magnetite-rich dikes and show prominent volcanic features including flow banding, gas-escape tubes, pahoehoe textures, and columnar jointing (Henriquez and Martin, 1978; Naslund et al., 2002; Nyström et al., 2016). At Pasos Blancos, coarse mineralized diopside-magnetite-anhydrite (± apatite ± albite ± K-feldspar) veins (as much as 50 vol% magnetite) crosscut highly altered andesite and cap subvertical lenses of massive magnetite (Naranjo et al., 2010). The veins show distinctive zonation, with diopside-rich margins and anhydrite-rich interiors. Late acid-sulfate and earlier alkali-calcic alteration

*E-mail: steelema@ualberta.ca

[1]Supplemental Material. Additional details on the geologic setting, analytical methods and results, Figures S1–S6, and Tables S1 and S2. Please visit https://doi.org/10.1130/GEOL.S.14470836 to access the supplemental material, and contact editing@geosociety.org with any questions.

CITATION: Bain, W.M., et al., 2021, Evidence for iron-rich sulfate melt during magnetite(-apatite) mineralization at El Laco, Chile: Geology, v. 49, p. 1044–1048, https://doi.org/10.1130/G48861.1

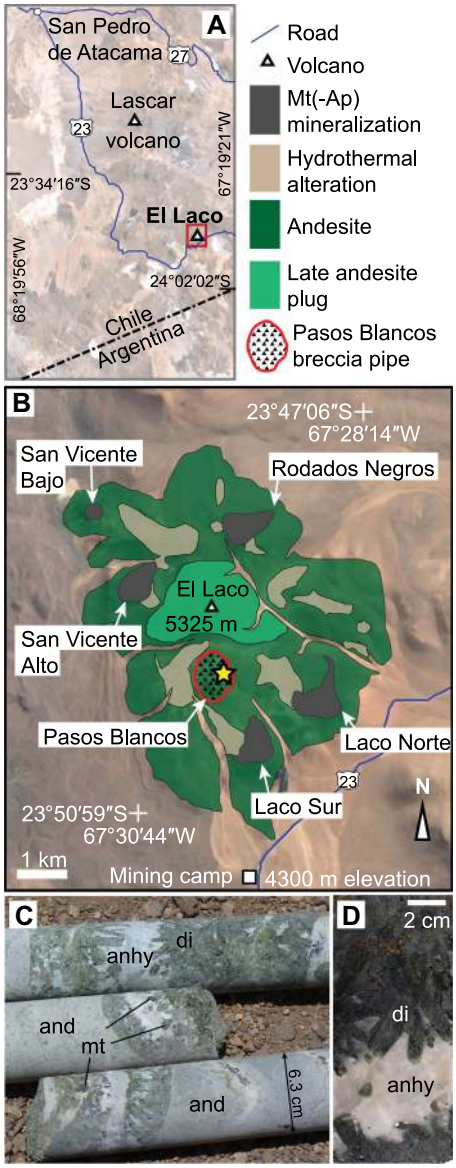

Figure 1. (A) Location of El Laco and Lascar volcano in northern Chile (on Google Earth™ image). (B) Geologic map (after Tornos et al., 2016) of El Laco (on Google Earth™ image). Yellow star is location of drill hole LCO-0932, drilled by by Compañía Minera del Pacífico (CMP) in 2009. (C) Example of diopside-magnetite-anhydrite (di-mt-anhy) vein in drill core (and—andesite). (D) Cut drill core (LCO-2014-205, drilled by Compañía Minera del Pacífico in 2014; 324.9 m) showing diopside-magnetite-anhydrite vein.

overprints ~30%–40% of the El Laco system (Tornos et al., 2017) and includes vast quantities of anhydrite and gypsum, which occur as stockwork veins, mounds, and sulfate-rich zones.

INCLUSION PETROGRAPHY AND MICROTHERMOMETRY

Inclusions were characterized by petrography, microthermometry, Raman spectroscopy, and scanning electron microscope–energy dispersive spectroscopy (SEM-EDS). Details of the analyses are described in the Supplemental Material. Our analyses focused on coeval magnetite, diopside, and lesser albite and apatite from ore-stage veins at Pasos Blancos (Fig. 1C; Table S1). All four minerals in all samples studied contain assemblages of primary inclusions composed of polycrystalline aggregates of translucent and opaque crystals at ambient temperature (Figs. 2A–2C; Fig. S3 in the Supplemental Material). Aqueous liquid-rich inclusions are conspicuously absent from all assemblages.

Phases and volumetric ratios are remarkably consistent within a given assemblage and always include anhydrite, hematite (5–15 vol%), and albite (Figs. 2D and 2H). Hematite likely represents oxidation of primary magnetite owing to outward diffusion of hydrogen (Mavrogenes and Bodnar, 1994). Paragenetically early assemblages in the cores of diopside and magnetite grains along the vein margins are notably more silica rich (based on modal proportions of phases), with anhydrite + hematite ± apatite constituting ~50 vol% of each inclusion, and albite + K-feldspar + quartz making up the remaining ~50 vol% (Figs. 2E–2H). Paragenetically later inclusions in the rims of diopside grains are dominated by anhydrite (as much as ~80 vol%), hematite, and alkali-sulfates including glauberite [$Na_2Ca(SO_4)_2$] (Fig. 2D). Both the earlier and later varieties of inclusions are primary and hosted in coeval magnetite and diopside, and thus represent ore-stage fluids. Additional phases consistently observed in the polycrystalline inclusions include pyrite (Fig. S4B), natrite (Na_2CO_3; Fig. 2D), allanite (Fig. S4), ilmenite (Fig. 2H), and halite, along with a vapor phase that occupies interstitial space between grains (10–20 vol%; Figs. 2B and 2C). Polycrystalline inclusions also occur alongside coeval vapor-rich inclusions in secondary assemblages that crosscut diopside grains. The secondary polycrystalline inclusions show the same phase assemblage as the primary inclusions in the diopside rims. The vapor-rich inclusions show no detectable molecular gases (e.g., CO_2, CH_4) and likely represent a low-density aqueous vapor present only in the late stages.

Primary and secondary assemblages of polycrystalline inclusions show consistent melting behavior within a given assemblage (Fig. 3; Fig. S6, Table S2). The onset of melting is between 400 and 470 °C, and commonly the first appearance of liquid allows the vapor phase (interstitial at ambient temperature [*T*]) to coalesce into a spherical bubble (Fig. 3). With continued heating, the translucent crystals progressively shrink, leading to final melting of silicate + sulfate between 694 and 769 °C in primary inclusions and between 700 and 784 °C in secondary inclusions. Within a given assemblage, the maximum range in final melting *T* never exceeds 47 °C. Complete melting of the opaque phases occurs within 50 °C of the last melting *T* of the translucent crystals. Liquid-vapor homogenization is between 800 and 951 °C, overlapping the range of *T* estimated from oxygen-isotope fractionation in the diopside-magnetite-anhydrite veins (900–1125 °C; Tornos et al., 2016).

DISCUSSION AND CONCLUSION

The polycrystalline inclusions represent an Fe-rich sulfate-silicate melt (e.g., ~6–17 wt% Fe, ~7–14 wt% Si, ~9–11 wt% S, based on volumetric proportions of mineral phases present). These inclusions occur along growth zones and show consistent phase assemblages, phase ratios, and melting behavior. Sulfate melts are stable at *T* as low as 900 °C in the system Na_2SO_4-$CaSO_4$ (Freyer et al., 1998), represented by the subsolidus assemblage of anhydrite plus glauberite (Fig. 2D). Addition of NaCl and H_2O significantly lowers the minimum melting *T* in this system (Walter et al., 2020, their figure 3), and addition of silica greatly enhances sulfate melting down to <400 °C (Cui et al., 2020). All of these factors are consistent with the inclusions observed here (Fig. 2E). Hence, the diopside-magnetite-anhydrite veins were generated by an Fe-sulfate-rich melt. This melt contained a significant component of felsic silicate material, evinced by the presence of plagioclase, K-feldspar, and quartz in paragenetically earlier inclusions (Figs. 2E–2H). This suggests that the melt evolved toward a sulfate-dominant composition over time (Figs. 2B–2D), likely as a result of fractional crystallization of silicate minerals and magnetite.

Anhydrite-bearing inclusions have been previously observed in pyroxene from hydrothermally altered andesite at El Laco and were interpreted as "hydrous saline melts" that condensed from a hydrothermal brine (Sheets, 1997; Broman et al., 1999). The anhydrite-rich inclusions described here, however, are hosted in ore-stage minerals and provide additional constraints that argue against derivation from an aqueous fluid. Firstly, if the sulfate melt formed by immiscible separation from an aqueous liquid, we would expect to see aqueous liquid–rich inclusions alongside the polycrystalline inclusions throughout the paragenesis. Instead, we find that aqueous liquid–rich inclusions are absent, and vapor-rich inclusions occur only in paragenetically later secondary assemblages. Secondly, the sulfate-rich inclusions contain no hydrous minerals or liquid H_2O but host significant proportions of anhydrous silicate and Fe-rich minerals (hematite, ilmenite, pyrite), inconsistent with condensation from an aqueous fluid. As such, our results indicate that the sulfate-rich melt was an orthomagmatic liquid, which degassed aqueous vapor late in the paragenesis.

Iron and other transition metals are highly soluble and strongly partitioned into sulfate-rich liquids (Lovering, 1982; Veksler et al., 2012; Cui et al., 2020). The iron contents of

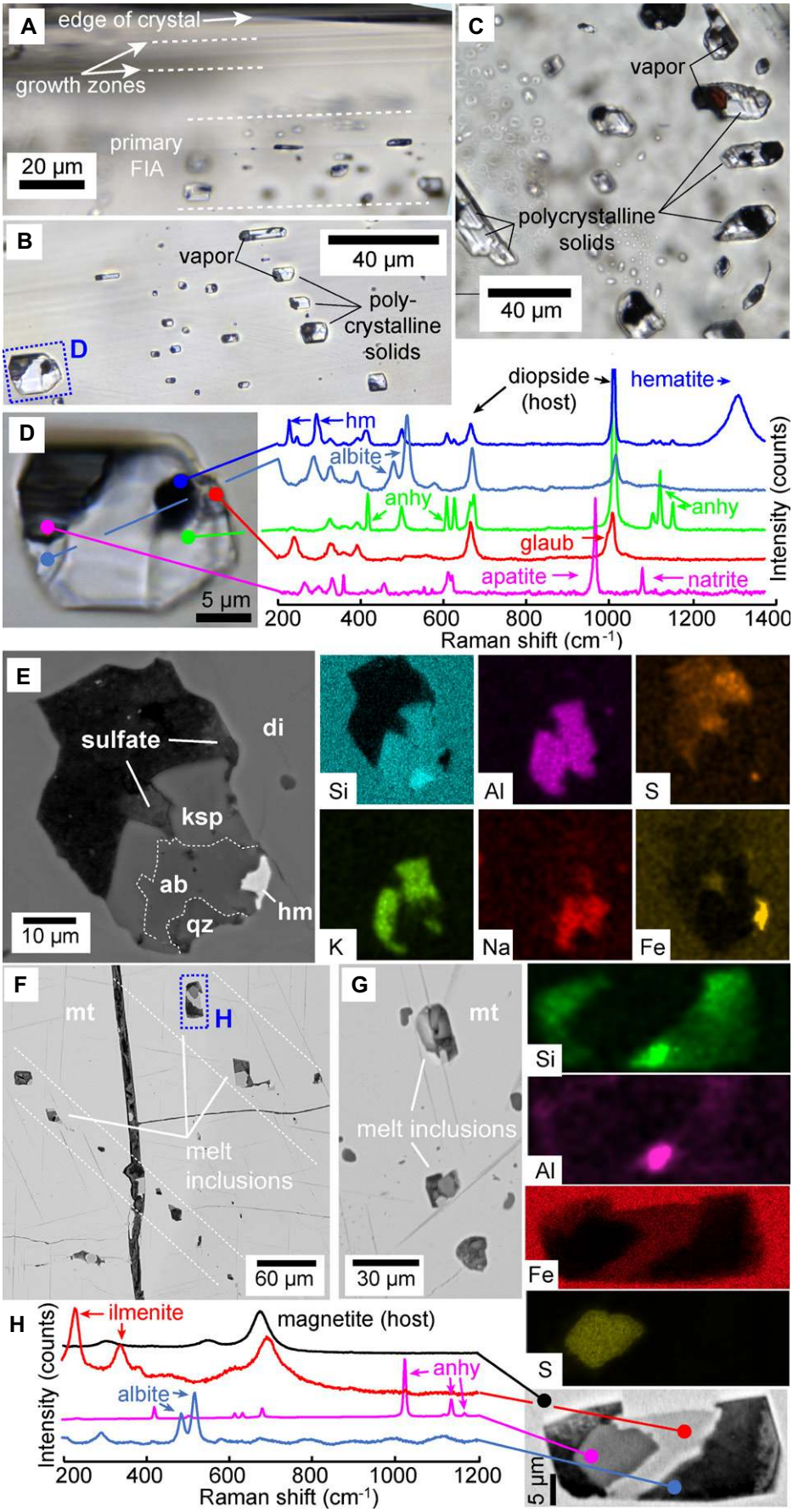

Figure 2. (A–C) Plane-polarized, transmitted light photomicrographs of primary polycrystalline inclusions in diopside. FIA—fluid inclusion assemblage. (D) Raman spectra of phases within polycrystalline inclusion shown in B. hm—hematite; anhy—anhydrite; glaub—glauberite. (E) Back-scattered electron image of diopside-hosted (di) inclusion and corresponding X-ray maps. Inclusion contains K-feldspar (ksp), albite (ab), quartz (qz), hematite (hm), and anhydrite (the latter of which completely filled upper void space prior to polishing). (F,G) Polycrystalline inclusions in magnetite. (H) Raman spectra and X-ray maps of magnetite-hosted inclusion shown in F.

the inclusions reported here are ~6–17 wt% Fe, implying that the sulfate melt was capable of depositing magnetite. This is confirmed by the occurrence of primary sulfate-rich inclusions in the magnetite itself (Figs. 2F–2H). Considering that the diopside-hosted inclusions occur in veins that cap massive magnetite, we posit that the initial Fe contents of the melt were >17 wt%, prior to extensive fractional crystallization of magnetite. Sulfate in the melt likely served as a local oxidant (evinced by the common occurrence of sulfides in the inclusions; Fig. S3B) and contributed to the oxidized nature of the Mt(-Ap) ore.

We contend that the most likely source of sulfate is anatexis and/or assimilation of evaporite-bearing strata by the intruding andesitic magma (Fig. 4). While no carbonate or evaporite rocks crop out at El Laco, several sulfate-rich units of the Salta Group (Yacoraite Formation, Caracoles Group, and Arizaro Formation) are exposed to the east and west of the complex and likely extend laterally beneath El Laco (Matthews et al., 1994, 1996; Scheuber et al., 2006). Several lines of evidence point to assimilation of sedimentary rock at El Laco, including crustal signatures of Sr-Nd isotopes in the ores; mixed magmatic-hydrothermal and external S isotopes from the diopside-magnetite-anhydrite veins; O isotopes from gypsum in Pasos Blancos identical to those of the Yacoraite Formation (Matthews et al., 1996; Tornos et al., 2017); and sedimentary xenoliths in the eruptive products of both El Laco (Naranjo et al., 2010) and the nearby Lascar volcano (Matthews et al., 1996). Our suggestion of a sedimentary component to the ore-forming fluid is broadly consistent with the recent work by Mungall et al. (2018), who suggested that Paleozoic phosphatic siderite ironstones that underlie the Salta Group were likely assimilated and contributed Fe (as well as P and CO_3^{2-}) to this system. While Fe isotopes of magnetite and pyrite suggest an andesitic source of Fe (Bilenker et al., 2016), they do not preclude a sedimentary source (Beard

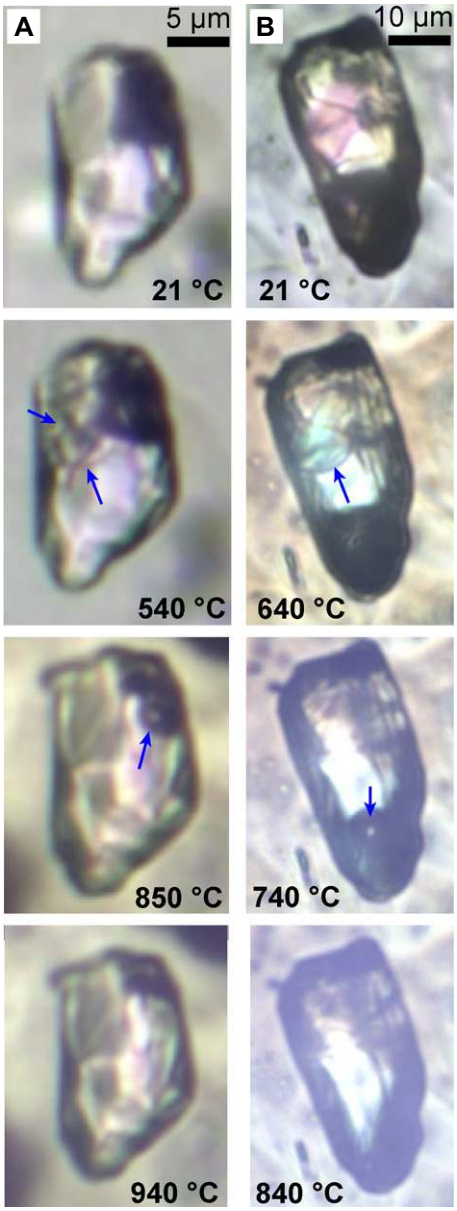

Figure 3. Phase changes in polycrystalline inclusions in diopside at high temperature. Arrows denote changes indicative of melting.

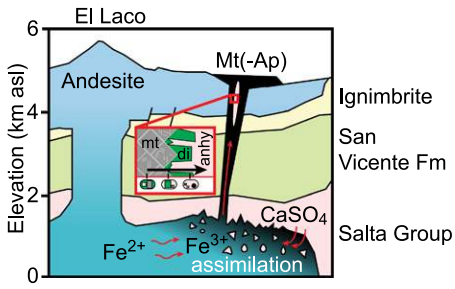

Figure 4. Schematic cross section (after Tornos et al., 2016) showing andesitic melt assimilating evaporite-bearing rocks and Fe^{3+} partitioning into sulfate-rich melt. Injections of this melt form magnetite orebodies by crystallization of magnetite (mt; gray) and diopside (di; green). Fractional crystallization drives the melt toward sulfate (anhydrite [anhy]; pink)–dominated composition, leading to formation of sulfate-rich veins and alteration. asl—above sea level; Fm—Formation. Inset shows a magnified view of the sulfate-rich veins, showing a temporal sequence (represented by the arrow) from early magnetite and diopside to later anhydrite. Relative proportions of these phases in primary melt inclusions are shown schematically.

et al., 2003), and both sedimentary and igneous sources of Fe are permissible.

We suggest that sulfate was added to the andesitic melt either by anatexis and mixing or by direct assimilation of sulfate evaporites (Fig. 4). This produced the composite sulfate-silicate liquid recorded by paragenetically early inclusions in the cores of diopside crystals. Contamination of andesitic liquid by addition of sulfate is supported by the modal proportions of minerals in the inclusions because the silicate portion (quartz, K-feldspar, and plagioclase) sums to an approximately andesitic composition. Addition of sulfate drove enrichment of oxidized Fe, either by partitioning from the andesitic melt or by leaching and/or assimilation of Fe-bearing sedimentary rocks, giving rise to more Fe-rich compositions and possibly also contributing to the separation of an immiscible Fe-rich liquid (Tornos et al., 2016; Mungall et al., 2018). The sulfate-dominant melts later in the paragenesis either evolved from this earlier sulfate-silicate melt by fractional crystallization or represent portions of anatectic sulfate liquid that did not mix with the andesitic melt. Fractional crystallization is supported by the paragenesis of the veins, which show diopside-magnetite-rich margins and nearly monomineralic anhydrite centerlines. In either case, flux of this later, sulfate-rich liquid through the El Laco complex resulted in formation of sulfate-rich veins and mounds at shallow levels and development of late acid-sulfate alteration by interaction with groundwater.

Our results point to sulfate-rich melts driving magnetite mineralization in the diopside-magnetite-anhydrite veins at El Laco. This agrees well with recent results from other Mt(-Ap) deposits that showed evidence for carbonate-sulfate melts (Panina and Motorina, 2008; Nikolenko et al., 2018; Bain et al., 2020). Thus, our results point to similar processes, whereby liquids dominated by sulfate or carbonate are produced by assimilation of evaporites and/or carbonates by mafic to intermediate silicate melts. This is also in accord with recent studies of triple O isotopes in Mt(-Ap) deposits, which indicate interaction between magmatic fluids, evaporites, and carbonate rocks (Peters et al., 2020). These results do not preclude the influence of other fluid(s) or processes in forming the range of mineralization styles at El Laco or other Mt(-Ap) deposits, but provide evidence for a key role of sulfate-rich melts as part of the ore-forming process. This implies that evaporites intruded by mafic to intermediate magmas should be considered a useful exploration indicator in the search for new Mt(-Ap) deposits.

ACKNOWLEDGMENTS

We thank our colleagues at Compañía Minera del Pacífico (CMP, Chile) for providing access to drill core. This work was supported by the Natural Sciences and Engineering Research Council of Canada (NSERC) through a Discovery Grant to M. Steele-MacInnis, and by project RTI2018-099157-A-I00 (MCI/AEI/FEDER, UE [Ministerio de Ciencia y Tecnología / Agencia Española de Investigación / Fondos Europeos de Desarrollo regional / Union Europea]) to F. Tornos. We thank two anonymous reviewers, Bob Bodnar, Katy Evans, and editor Chris Clark for their constructive reviews that helped to significantly improve this paper.

REFERENCES CITED

Bain, W.M., Steele-MacInnis, M., Li, K., Li, L., Mazdab, F.K., and Marsh, E., 2020, A fundamental role of carbonate-sulfate melts in formation of iron oxide-apatite deposits: Nature Geoscience, v. 13, p. 751–757, https://doi.org/10.1038/s41561-020-0635-9.

Beard, B.L., Johnson, C.M., Von Damm, K.L., and Poulson, R.L., 2003, Iron isotope constraints on Fe cycling and mass balance in oxygenated Earth oceans: Geology, v. 31, p. 629–632, https://doi.org/10.1130/0091-7613(2003)031<0629:IICOFC>2.0.CO;2.

Bilenker, L.D., Simon, A.C., Reich, M., Lundstrom, C.C., Gajos, N., Bindeman, I., Barra, F., and Munizaga, R., 2016, Fe-O stable isotope pairs elucidate a high-temperature origin of Chilean iron oxide-apatite deposits: Geochimica et Cosmochimica Acta, v. 177, p. 94–104, https://doi.org/10.1016/j.gca.2016.01.009.

Boso, M.A., and Monaldi, C.R., 1990, Oolitic stratabound iron ores in the Silurian of Argentina and Bolivia, *in* Fontboté, L., et al., eds., Stratabound Ore Deposits in the Andes: Society for Geology Applied to Mineral Deposits Special Publication 8, p. 175–186, https://doi.org/10.1007/978-3-642-88282-1_11.

Broman, C., Nyström, J.O., Henríquez, F., and Elfman, M., 1999, Fluid inclusions in magnetite-apatite ore from a cooling magmatic system at El Laco, Chile: GFF (Journal of the Geological Society of Sweden), v. 121, p. 253–267, https://doi.org/10.1080/11035899901213253.

Cui, H., Zhong, R., Xie, Y., Yuan, X., Liu, W., Brugger, J., and Yu, C., 2020, Forming sulfate- and REE-rich fluids in the presence of quartz: Geology, v. 48, p. 145–148, https://doi.org/10.1130/G46893.1.

Freyer, D., Voigt, W., and Köhnke, K., 1998, The phase diagram of the systems Na_2SO_4-$CaSO_4$: European Journal of Solid State and Inorganic Chemistry, v. 35, p. 595–606, https://doi.org/10.1016/S0992-4361(99)80001-0.

Harmon, R.S., Barreiro, B.A., Moorbath, S., Hoefs, J., Francis, P.W., Thorpe, R.S., Déruelle, B., McHugh, J., and Viglino, J.A., 1984, Regional O-, Sr-, and Pb-isotope relationships in late Cenozoic calc-alkaline lavas of the Andean Cordillera: Journal of the Geological Society, v. 141, p. 803–822, https://doi.org/10.1144/gsjgs.141.5.0803.

Henríquez, F., and Martin, R.F., 1978, Crystal-growth textures in magnetite flows and feeder dykes, El Laco, Chile: Canadian Mineralogist, v. 16, p. 581–589.

Hildebrand, R.S., 1986, Kiruna-type deposits: Their origin and relationship to intermediate subvolcanic plutons in the Great Bear magmatic zone,

Northwest Canada: Economic Geology and the Bulletin of the Society of Economic Geologists, v. 81, p. 640–659, https://doi.org/10.2113/gsecongeo.81.3.640.

Knipping, J.L., Bilenker, L.D., Simon, A.C., Reich, M., Barra, F., Deditius, A.P., Lundstrom, C., Bindeman, I., and Munizaga, R., 2015, Giant Kiruna-type deposits form by efficient flotation of magmatic magnetite suspensions: Geology, v. 43, p. 591–594, https://doi.org/10.1130/G36650.1.

Lovering, D.G., 1982, Molten Salt Technology: New York, Springer, 533 p., https://doi.org/10.1007/978-1-4757-1724-2.

Marquillas, R.A., del Papa, C., and Sabino, I.F., 2005, Sedimentary aspects and paleoenvironmental evolution of a rift basin: Salta Group (Cretaceous–Paleogene), northwestern Argentina: International Journal of Earth Sciences, v. 94, p. 94–113, https://doi.org/10.1007/s00531-004-0443-2.

Matthews, S.J., Jones, A.P., and Beard, A.D., 1994, Buffering of melt oxygen fugacity by sulphur redox reactions in calc-alkaline magmas: Journal of the Geological Society, v. 151, p. 815–823, https://doi.org/10.1144/gsjgs.151.5.0815.

Matthews, S.J., Marquillas, R.A., Kemp, A.J., Grange, F.K., and Gardeweg, M.C., 1996, Active skarn formation beneath Lascar Volcano, northern Chile: A petrographic and geochemical study of xenoliths in eruption products: Journal of Metamorphic Geology, v. 14, p. 509–530, https://doi.org/10.1046/j.1525-1314.1996.00359.x.

Mavrogenes, J.A., and Bodnar, R.J., 1994, Hydrogen movement into and out of fluid inclusions in quartz: Experimental evidence and geologic implications: Geochimica et Cosmochimica Acta, v. 58, p. 141–148, https://doi.org/10.1016/0016-7037(94)90452-9.

Mungall, J.E., Long, K., Brenan, J.M., Smythe, D., and Naslund, H.R., 2018, Immiscible shoshonitic and Fe-P-oxide melts preserved in unconsolidated tephra at El Laco volcano, Chile: Geology, v. 46, p. 255–258, https://doi.org/10.1130/G39707.1.

Naranjo, J.A., Henríquez, F., and Nyström, J.O., 2010, Subvolcanic contact metasomatism at El Laco Volcanic Complex, Central Andes: Andean Geology, v. 37, p. 110–120, https://doi.org/10.4067/S0718-71062010000100005.

Naslund, H.R., Henríquez, F., Nyström, J.O., Vivallo, W., and Dobbs, F.M., 2002, Magmatic iron ores and associated mineralisation: Examples from the Chilean High Andes and Coastal Cordillera, *in* Porter, T.M., ed., Hydrothermal Iron Oxide Copper-Gold & Related Deposits: A Global Perspective: Adelaide, PGC Publishing, v. 2, p. 207–226.

Nikolenko, A.M., Redina, A.A., Doroshkevich, A.G., Prokopyev, I.R., Ragozin, A.L., and Vladykin, N.V., 2018, The origin of magnetite-apatite rocks of Mushgai-Khudag Complex, South Mongolia: Mineral chemistry and studies of melt and fluid inclusions: Lithos, v. 320–321, p. 567–582, https://doi.org/10.1016/j.lithos.2018.08.030.

Nyström, J.O., and Henriquez, F., 1994, Magmatic features of iron ores of the Kiruna type in Chile and Sweden: Ore textures and magnetite geochemistry: Economic Geology and the Bulletin of the Society of Economic Geologists, v. 89, p. 820–839, https://doi.org/10.2113/gsecongeo.89.4.820.

Nyström, J.O., Henríquez, F., Naranjo, J.A., and Naslund, H.R., 2016, Magnetite spherules in pyroclastic iron ore at El Laco, Chile: American Mineralogist, v. 101, p. 587–595, https://doi.org/10.2138/am-2016-5505.

Panina, L.I., and Motorina, I.V., 2008, Liquid immiscibility in deep-seated magmas and the generation of carbonatite melts: Geochemistry International, v. 46, p. 448–464, https://doi.org/10.1134/S0016702908050029.

Peters, S.T.M., Alibabaie, N., Pack, A., McKibbin, S.J., Raeisi, D., Nayebi, N., Torab, F., Ireland, T., and Lehmann, B., 2020, Triple oxygen isotope variations in magnetite from iron-oxide deposits, central Iran, record magmatic fluid interaction with evaporite and carbonate host rocks: Geology, v. 48, p. 211–215, https://doi.org/10.1130/G46981.1.

Rhodes, A.L., and Oreskes, N., 1999, Oxygen isotope composition of magnetite deposits at El Laco, Chile: Evidence of formation from isotopically heavy fluids, in Skinner, B.J., ed., Geology and Ore Deposits of the Central Andes: Society of Economic Geologists Special Publication 7, p. 333–351, https://doi.org/10.5382/SP.07.11.

Richards, J.P., and Villeneuve, M., 2001, The Llullaillaco volcano, northwest Argentina: Construction by Pleistocene volcanism and destruction by sector collapse: Journal of Volcanology and Geothermal Research, v. 105, p. 77–105, https://doi.org/10.1016/S0377-0273(00)00245-6.

Scheuber, E., Mertmann, D., Ege, H., Silva-González, P., Heubeck, C., Reutter, K.-J., and Jacobshagen, V., 2006, Exhumation and basin development related to formation of the Central Andean Plateau, 21°S, *in* Oncken, O., et al., eds., The Andes: Active Subduction Orogeny: Berlin, Springer, p. 285–301, https://doi.org/10.1007/978-3-540-48684-8_13.

Sheets, S.A., 1997, Fluid inclusion study of the El Laco magnetite deposits, Chile [M.S. thesis]: Hanover, New Hampshire, Dartmouth College, 94 p.

Sillitoe, R.H., and Burrows, D.R., 2002, New field evidence bearing on the origin of the El Laco magnetite deposit, northern Chile: Economic Geology and the Bulletin of the Society of Economic Geologists, v. 97, p. 1101–1109, https://doi.org/10.2113/gsecongeo.97.5.1101.

Simon, A.C., Knipping, J., Reich, M., Barra, F., Deditius, A.P., Bilenker, L., and Childress, T., 2018, Kiruna-type iron oxide-apatite (IOA) and iron oxide copper-gold (IOCG) deposits form by a combination of igneous and magmatic-hydrothermal processes: Evidence from the Chilean Iron Belt, *in* Arribas R., A.M., and Mauk, J.L., eds., Metals, Minerals, and Society: Society of Economic Geologists Special Publication 21, p. 89–114, https://doi.org/10.5382/SP.21.06.

Tornos, F., Velasco, F., and Hanchar, J.M., 2016, Iron-rich melts, magmatic magnetite, and superheated magmatic-hydrothermal systems: The El Laco deposit, Chile: Geology, v. 44, p. 427–430, https://doi.org/10.1130/G37705.1.

Tornos, F., Velasco, F., and Hanchar, J.M., 2017, The magmatic to magmatic-hydrothermal evolution of the El Laco deposit (Chile) and its implications for the genesis of magnetite-apatite deposits: Economic Geology and the Bulletin of the Society of Economic Geologists, v. 112, p. 1595–1628, https://doi.org/10.5382/econgeo.2017.4523.

Veksler, I.V., Dorfman, A.M., Dulski, P., Kamenetsky, V.S., Danyushevsky, L.V., Jeffries, T., and Dingwell, D.B., 2012, Partitioning of elements between silicate melt and immiscible fluoride, chloride, carbonate, phosphate and sulfate melts, with implications to the origin of natrocarbonatite: Geochimica et Cosmochimica Acta, v. 79, p. 20–40, https://doi.org/10.1016/j.gca.2011.11.035.

Velasco, F., Tornos, F., and Hanchar, J.M., 2016, Immiscible iron- and silica-rich melts and magnetite geochemistry at the El Laco volcano (northern Chile): Evidence for a magmatic origin for the magnetite deposits: Ore Geology Reviews, v. 79, p. 346–366, https://doi.org/10.1016/j.oregeorev.2016.06.007.

Walter, B.F., Steele-MacInnis, M., Giebel, R.J., Marks, M.A.W., and Markl, G., 2020, Complex carbonate-sulfate brines in fluid inclusions from carbonatites: Estimating compositions in the system H_2O-Na-K-CO_3-SO_4-Cl: Geochimica et Cosmochimica Acta, v. 277, p. 224–242, https://doi.org/10.1016/j.gca.2020.03.030.

Printed in USA